Heat and Mass Transfer 38 (2002) 695–704 © Springer-Verlag 2001
DOI 10.1007/s002310100274

A numerical study of heat transfer of a porous block with the random porosity model in a channel flow

W. S. Fu, S. F. Chen

Abstract In this paper, heat transfer of a hot plate with a porous block in a channel flow is numerically investigated. A porous block is simulated as a fin type heat sink. The random/artificial porosity models are used to generate the distribution of porosity. In fact, the distribution of porosity in porous medium is irregular, thus the random porosity model is more realistic than the constant or variable porosity model to describe the phenomena happening in porous medium. Therefore, the distribution of porosity of porous block obeys the random porosity model, and the factors of mean porosity and standard deviation are taken into consideration. The variations of the porosity and the velocity in porous block are no longer smooth. For obtaining more heat transfer rate, the artificial porosity model is proposed. The heat transfer rates of the several cases derived by the artificial porosity model are better than those of the random porosity model. The thermal performance of porous block is larger than that of solid block as the mean porosity is larger than 0.5.

List of symbols

C_f	specific heat of fluid, J kg^{-1} K^{-1}
D_p	dimensionless mean bead diameter, d_p/h
d_p	mean bead diameter, m
F	inertial factor
h	dimensionless distance from the jet inlet to the top surface of the block
h_p	dimensionless height of the block
h_x	local heat transfer coefficient, W m^{-2} K^{-1}
K	permeability, m^2
k	thermal conductivity, W m^{-1} K^{-1}
l_p	dimensionless length of the block, l_p/h
$N(a, b^2)$	normal distribution with mean a and standard deviation b
Nu	local Nusselt number along the heated wall of the block
$\overline{\mathrm{Nu}}$	mean Nusselt number
P	dimensionless pressure
Pr	Prandtl number, ν/α
p	pressure, N m^{-2}
Re	Reynolds number, $u_0 h/\nu_f$
T	temperature, K
U	dimensionless velocity in the X direction, u/u_0
u	velocity in the x direction, m s^{-1}
u_0	maximum inlet velocity, m s^{-1}
V	dimensionless velocity in the Y direction, v/u_0
v	velocity in the y direction, m s^{-1}
X, Y	dimensionless Cartesian coordinates, x/h, y/h
x, y	Cartesian coordinates, m
$\|\ \|$	magnitude of velocity vector

Greek symbols

α	thermal diffusivity, m^2 s^{-1}
$\bar{\varepsilon}$	mean porosity
μ	viscosity, kg m^{-1} s^{-1}
ν	kinematic viscosity, m^2 s^{-1}
θ	dimensionless temperature
ρ	density, kg m^{-3}
σ_ε	standard deviation of porosity
Φ	computational variable
ψ	dimensionless stream function

Superscripts

n	the nth iteration index
$\bar{}$	mean value
$\rightarrow$	velocity vector

Subscripts

C.V.	control volume
e	effective value
f	external flow field
i	index; inlet
p	porous block
s	solid block
w	solid wall
X	along the X direction

Received on 5 March 2001 / Published online: 29 November 2001

W. S. Fu (✉), S. F. Chen
Department of Mechanical Engineering
National Chiao Tung University
1001Ta Hsueh Road, Hsinchu 30010, Taiwan

The support of this work by National Science Council, Taiwan, R.O.C under contract NSC87-2212-E-009-035 is gratefully acknowledged.

1 Introduction

Recently a pin fin heat sink which is an indispensable thermal dissipation device shown in Fig. 1a is widely applied in electrical cooling system. Due to the complex geometry of the pin fin heat sink, an appropriate method adopted to analyze the heat transfer characteristics of the pin fin heat sink has been hardly proposed. However, from a macropoint view, the pin fin heat sink can be approximately regarded as a kind of porous medium. Therefore,

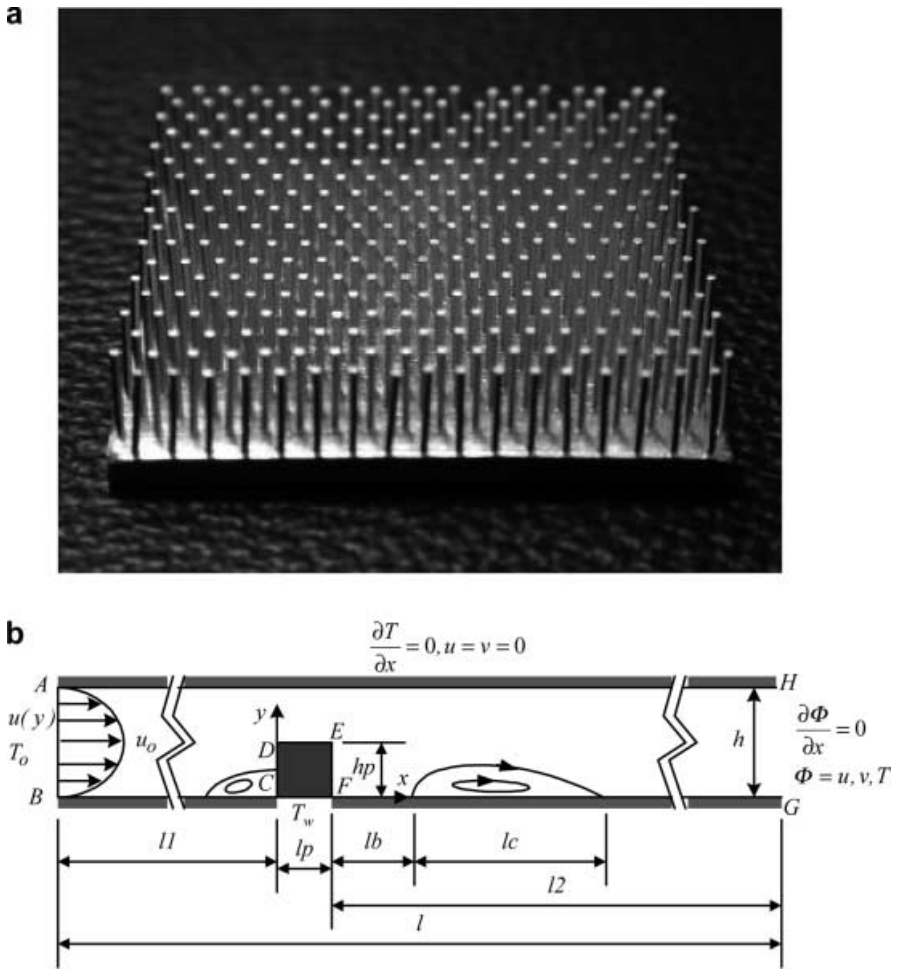

Fig. 1. **a** Pin fin heat sink. **b** Physical model

that the results obtained from analyzing the porous medium simulate the results of the pin fin heat sink is worth studying.

For facilitating the analysis, the porosity of the porous medium was usually assumed as constant, called a constant porosity model. However, Roblee et al. [1] and Benenati and Brosilow [2] based on their experimental results observed the porosity varied significantly in the near wall region. Schwartz et al. [3] conducted experimental studies and measured the maximum velocity which is normally called channelling effect in the near wall region. These phenomena directly validated that the porosity regarded as a variable was more realistic. Cheng et al. [4] pointed out that in lot of literature the porosity was simulated as a damped oscillatory function of the distance from the wall and the damped oscillatory phenomenon was insignificant as the distance was larger than five bead diameters for packed beds. Therefore, the variation of the porosity is assumed as an exponential function of the distance from the solid wall and is called a variable porosity model. Based upon the above experiences, up to now two different models are adopted to derive the individual equations of fluid flow and heat transfer for the porous medium.

However, Georgiadis et al. [5–7] studied the unidirectional flow and heat transport phenomena in the random porous medium. The results indicated the mean flow rate $U(\varepsilon)$ based on the random porosity was larger than that $U(\bar{\varepsilon})$ based on the constant porosity when the Forchheimer model of flow was held. Saito et al. [8] studied the effects of the porosity and void distributions on the permeability by direct simulation Monte Carlo method and found that the permeability depended not only on the porosity but also on the void distribution strongly. These facts indicated that except for special screen process the sizes of the beads are extremely difficult to be uniform. In fact, the distribution of porous medium is difficult to obey the distributions of the constant or variable porosity model mentioned above. That the porosity in porous medium is irregular or random is more realistic, this distribution of porosity is conveniently named a random porosity model. Although the effect of the random porosity distribution on the flow field had been discussed in the past, however, most of previous studies only concentrated on special physical phenomena. Fu and Huang [9] studied flow and thermal fields of a porous block with the random porosity distribution under a laminar slot impinging jet. The results showed that the porosity near the heat wall should be smaller to enhance heat transfer rate for an impinging jet flow. Based on the results of the above literature, for obtaining more efficient performance of the use of porous medium, the distribution of porosity in porous medium need to be arranged appropriately. This special arrangement of the distribution of porosity in porous block is briefly called artificial porosity model. Besides, for expending the application of porous medium

more widely, utilization of porous block to simulate a fin type dissipation device (heat sink) which is usually mounted on a hot component is proposed.

Therefore, the purpose of this paper is to investigate heat transfer characteristics of a porous block mounted on a hot plate in a channel flow numerically. Corresponding to a realistic situation, the distributions of porosity of porous block are derived by the random porosity model. In addition, for enhancing the heat transfer rate of porous block, the distributions of porosity derived by the artificial porosity model are also studied.

2 Physical description

The physical model is shown in Fig. 1b. There is a two-dimensional laminar channel flow. A porous block is mounted on a hot plate. The height of the channel is h. The length l_p and height h_p of the porous block are same and equal to $h/2$. The inlet velocity distribution $u(y)$ of the flow is fully developed and the inlet temperature T_0 of the fluid is constant. The length of the hot plate is l_p, and the temperature of this region is T_w which is higher than T_0. Expect the hot plate, the other wall regions are insulated. The distribution of porosity is derived by the random porosity model. The whole computation domain is large enough for the fully developed distributions of the velocity and temperature at the outlet ($l_1 = 8h_p$ and $l_2 = 80h_p$). Under this configuration, the flow field can be separated into two conjugate regions: one stands for the internal flow field of the porous block and the other is called the external flow field, which excludes the porous block.

In order to facilitate the analysis, the following assumptions are made.

(1) The flow field is steady, two-dimensional, single phase, laminar and incompressible.
(2) The cooling fluid is air and the thermophysical properties are constant based on $T_{ref} = T_0 + \frac{1}{3}(T_w - T_0)$ and the effect of gravity is neglected.
(3) The effective viscosity of the porous medium is equal to the viscosity of the external fluid.
(4) To enhance the thermal performance, the porous block is made of copper beads and the ratio of k_s/k_f is larger than 1.
(5) Permeability K and inertia factor F are obtained from the following Ergun equations recommended by Vafai [10].

$$K = \frac{\varepsilon^3 d_p^2}{150(1-\varepsilon)^2} \tag{1}$$

$$F = \frac{1.75}{\sqrt{150}\,\varepsilon^{1.5}} \tag{2}$$

(6) The effective thermal conductivity of porous block k_e is calculated by a following prediction equation proposed by Batchelor and O'Brien [11]. This equation which consists of the solid conductivity k_s and the fluid conductivity k_f is suitable for a high ratio of k_s/k_f and was validated experimentally by Shonnard and Whitaker [12].

$$\frac{k_e}{k_f} = (4 \cdot \ln\left(\frac{k_s}{k_f}\right) - 11) \tag{3}$$

Based on the above assumptions, the governing equations, boundary conditions and geometry dimensions are normalized in tension forms as follows:

Governing equations of the external flow field

Continuity equation:

$$\frac{\partial U_i^{\langle f\rangle}}{\partial X_j} = 0 \tag{4}$$

Momentum equation:

$$U_j^{\langle f\rangle}\frac{\partial U_i^{\langle f\rangle}}{\partial X_j} = -\frac{\partial P^{\langle f\rangle}}{\partial X_i} + \frac{1}{\mathrm{Re}}\frac{\partial^2 U_i^{\langle f\rangle}}{\partial X_j^2} \tag{5}$$

Energy equation:

$$U_j^{\langle f\rangle}\frac{\partial \theta^{\langle f\rangle}}{\partial X_j} = \frac{1}{\mathrm{Re}\cdot \mathrm{Pr_f}}\frac{\partial^2 \theta^{\langle f\rangle}}{\partial X_j^2} \tag{6}$$

The Brinkman–Forchheimer-extended Darcy model is used for the internal flow field for the porous block.

Continuity equation:

$$\frac{\partial U_i^{\langle p\rangle}}{\partial X_j} = 0 \tag{7}$$

Momentum equation:

$$U_j^{\langle p\rangle}\frac{\partial}{\partial X_j}\left(\frac{U_i^{\langle p\rangle}}{\varepsilon}\right) = -\frac{\partial P^{\langle p\rangle}}{\partial X_i} + \frac{1}{\mathrm{Re}}\frac{\partial^2 U_i^{\langle p\rangle}}{\partial X_j^2} - \frac{\varepsilon}{\mathrm{ReDa}}U_i^{\langle p\rangle} - \frac{F\varepsilon}{\sqrt{\mathrm{Da}}}\left|\vec{U}^{\langle p\rangle}\right|U_i^{\langle p\rangle} \tag{8}$$

Energy equation:

$$U_j^{\langle p\rangle}\frac{\partial \theta^{\langle p\rangle}}{\partial X_j} = \frac{\partial}{\partial X_j}\left(\frac{1}{\mathrm{Re}\cdot \mathrm{Pr_p}}\frac{\partial \theta^{\langle p\rangle}}{\partial X_j}\right) \tag{9}$$

where

$$X_i = x_i/h, \quad U_i^{\langle f\rangle} = u_i^{\langle f\rangle}/\bar{u}, \quad P^{\langle f\rangle} = P^{\langle f\rangle}/\rho\bar{u}^2 \ , \tag{10a}$$

$$U_i^{\langle p\rangle} = u_i^{\langle p\rangle}/\bar{u}, \quad P^{\langle p\rangle} = p^{\langle p\rangle}/\rho\bar{u}^2, \quad \mathrm{Re} = \bar{u}h/\nu_f \ , \tag{10b}$$

$$\mathrm{Da} = K/H^2, \quad \left|\vec{U}^{\langle p\rangle}\right| = \sqrt{U^2+V^2}^{\langle p\rangle} \ , \tag{10c}$$

$$\theta^{\langle f\rangle} = (T^{\langle f\rangle} - T_0)/(T_w - T_0), \quad \theta^{\langle p\rangle} = (T^{\langle p\rangle} - T_0)/(T_w - T_0) \ , \tag{10d}$$

$$\mathrm{Pr_f} = \nu_f/\alpha_f, \quad \mathrm{Pr_p} = \nu_p/\alpha_p, \quad \alpha_f = k_f/\rho_f C_f, \quad \alpha_p = k_e/\rho_f C_f \ . \tag{10e}$$

$\bar{u}$ is the mean inlet velocity, $\bar{u} = \frac{1}{h}\int_0^h u\,dy\Big|_{inlet}$

Boundary conditions
On the surfaces AH, BC, and FG:

$$U^{\langle f\rangle} = 0, \quad V^{\langle f\rangle} = 0, \quad \frac{\partial \theta^{\langle f\rangle}}{\partial Y} = 0 \ . \tag{11}$$

On the surface AB:

$$U^{\langle f\rangle} = -6(Y^2 - Y), \quad V^{\langle f\rangle} = 0, \quad \theta^{\langle f\rangle} = 0 \ . \tag{12}$$

On the surface HG:

$$\frac{\partial U^{\langle f\rangle}}{\partial X} = 0, \quad \frac{\partial V^{\langle f\rangle}}{\partial X} = 0, \quad \frac{\partial \theta^{\langle f\rangle}}{\partial X} = 0 \ . \tag{13}$$

On the surface CF:

$$U^{\langle p\rangle} = 0, \quad V^{\langle p\rangle} = 0, \quad \theta^{\langle p\rangle} = 1 \ . \tag{14}$$

Interfacial conditions
As for the interfacial conditions, according to Hadim [13], the continuity of each term of velocity, temperature, pressure, shear stress and heat flux at the fluid/porous block interfaces are satisfied and shown as follows.
At the fluid/porous medium interfaces CD and EF:

$$\begin{aligned} &U^{\langle f\rangle} = U^{\langle p\rangle}, \quad V^{\langle f\rangle} = V^{\langle p\rangle}, \quad P^{\langle f\rangle} = P^{\langle p\rangle}, \\ &\frac{\partial U^{\langle f\rangle}}{\partial X} = \frac{\partial U^{\langle p\rangle}}{\partial X}, \quad \frac{\partial V^{\langle f\rangle}}{\partial X} = \frac{\partial V^{\langle p\rangle}}{\partial X}, \\ &\theta^{\langle f\rangle} = \theta^{\langle p\rangle}, \quad k_f \frac{\partial \theta^{\langle f\rangle}}{\partial X} = k_e \frac{\partial \theta^{\langle p\rangle}}{\partial X} \ . \end{aligned} \tag{15}$$

At the fluid/porous medium interface DE:

$$\begin{aligned} &U^{\langle f\rangle} = U^{\langle p\rangle}, \quad V^{\langle f\rangle} = V^{\langle p\rangle}, \quad P^{\langle f\rangle} = P^{\langle p\rangle}, \\ &\frac{\partial U^{\langle f\rangle}}{\partial Y} = \frac{\partial U^{\langle p\rangle}}{\partial Y}, \quad \frac{\partial V^{\langle f\rangle}}{\partial Y} = \frac{\partial V^{\langle p\rangle}}{\partial Y}, \\ &\theta^{\langle f\rangle} = \theta^{\langle p\rangle}, \quad k_f \frac{\partial \theta^{\langle f\rangle}}{\partial Y} = k_e \frac{\partial \theta^{\langle p\rangle}}{\partial Y} \ . \end{aligned} \tag{16}$$

3 Numerical method

3.1 Numerical scheme and meshes

The SIMPLEC algorithm with TDMA solver is used to solve the governing equations (4)–(9) for the flow and thermal fields. Equations (4)–(9) are discretized into algebraic equations by using the control volume method. The under-relaxation factors are 0.3–0.5 for both the velocity and temperature fields. The staggered grids are used, and the finer meshes are placed in the front and rear regions of the porous block and the inlet/outlet regions. The non-uniform meshes with a scale ratio of 1.1 are adopted, and the uniform meshes are placed in the porous block. The harmonic mean formulation of thermophysical properties is used to avoid the effects of abrupt change of these properties across the interfacial regions of the porous block and external flow fields for the computation accuracy.

3.2 Procedure of the random porosity model

According to the results of the experimental works conducted by Fu and Huang [14], the porosity distribution of the porous medium approximately follows the form of the normal distribution with mean porosity $\bar{\varepsilon}$ and standard deviation σ_ε. For necessity of computing process, the theoretic form of the porosity distribution of the random porosity model is obtained from Kinderman–Ramage procedure [15], which is used to generate a random variable ξ of the standard normal distribution, $N(0,1)$, first. Moreover, the random variable ξ is transformed to gain a general random variable ε corresponding to a general normal distribution, $N(\bar{\varepsilon}, \sigma_\varepsilon^2)$, of which the mean $\bar{\varepsilon}$ and standard deviation σ_ε are equal to designed constants, respectively. Therefore, the distribution of the general random variable ε is regarded as the porosity distribution of the random porosity model and the mean porosity of the porosity distribution is $\bar{\varepsilon}$ in this study.

3.3 Computing parameters

Main parameters used in the study are tabulated in Table 1, including the Reynolds number Re mean porosity $\bar{\varepsilon}$, standard deviation σ_ε, mean diameter of beads D_p, Prandtl number Pr, height of porous block H_p, length L_p, temperature of inlet air θ_0 and temperature of hot plate θ_w.

The conservation residues of the equations of the momentum, energy and continuity and the relative error of each variable are used to examine the convergence criteria and are defined as follows.

$$\left(\sum \left| \text{Residue of } \Phi \text{ equation} \right|^2_{\text{C.V.}}\right)^{1/2} \le 10^{-4}, \quad \Phi = U, V \text{ and } \theta \ . \tag{17}$$

$$\frac{\max\left| \Phi^{n+1} - \Phi^{n} \right|}{\max\left| \Phi^{n+1} \right|} \le 10^{-5}, \quad \Phi = U, V, P \text{ and } \theta \tag{18}$$

3.4 Verification of numerical sheme

For selecting appropriate grid system in this channel flow, the results of grid tests are listed in Table 2, and 210×80 meshes in the total domain and 40×40 meshes in porous block are chosen.

Table 1. The main parameters

h (mm)	h_p (mm)	l_p (mm)	T_w (°C)	T_0 (°C)	H_p	L_p	D_p	Re	$\bar{\varepsilon}$	σ_ε (%)	Pr_f	Pr_p
30	15	15	80	20	0.5	0.5	0.1	500	0.5 0.7	5 10	0.7	0.026

Table 2. Grid tests for the case of Re = 500, $H_P = 0.5$, $L_P = 0.5$, $\bar{\varepsilon} = 0.5$, $\sigma_\varepsilon = 10\%$ and Pr = 0.7

Meshes of X (A + B + C)	Meshes of Y (D + E)	$\overline{Nu}$
162 (50 + 20 + 92)	40 (20 + 20)	47.95
192 (58 + 32 + 102)	64 (32 + 32)	47.76
144 (40 + 40 + 64)	80 (40 + 40)	47.61
168 (50 + 40 + 78)	80 (40 + 40)	47.61
210 (64 + 40 + 106)	80 (40 + 40)	47.62
172 (50 + 42 + 80)	84 (42 + 42)	47.66
214 (64 + 42 + 108)	84 (42 + 42)	47.68
184 (52 + 50 + 82)	100 (50 + 50)	47.12

In Fig. 2, to validate the accuracy of algorithm in this study, the experimental results of Schroeder [16] and numerical results of Cheng and Hsu [17] are used as bench mark solutions, and the results of this study are compared with those of them. The distributions of velocity and temperature are consistent well under the variable porosity model for $Re_p = 321$, $d_p/H = 0.37$, $\varepsilon = 0.4$, $k_s/k_f = 0.586$ and Pr = 7.0. The results of other situations compared with Hadim [14] and Vafai [10] had been validated in our previous work [18].

4 Results and discussion

4.1 Effects of the random porosity model

Since infinite patterns can be generated with a given mean porosity $\bar{\varepsilon}$ and standard deviation σ_ε, and it is difficult to solve all patterns. Therefore only several patterns with the mean porosities $\bar{\varepsilon}$ (=0.5 and 0.7) and standard deviations σ_ε (=5 and 10%) are presented to investigate the thermal performance of the porous block with the random porosity model.

The global porosity distribution maps and the distributions of local porosity ε_X along the X direction at $Y = 0.25$ of two selected cases (based on $\bar{\varepsilon} = 0.5$ and $\sigma_\varepsilon = 10\%$) are shown in Fig. 3a–c. In the global porosity distribution maps, the total area is approximately divided into several main different porosity regions with different colors and the darker color represents the smaller porosity. For the variable porosity model, the local porosity near the wall region is about unity. Oppositely, for the random porosity model, the porosity distributions are not in order, then the region between the material of porous block beads and the solid wall may not be definitely sparser than the other regions. The standard deviation σ_ε indicates the uniformity of the distribution. As a result, the higher the standard deviation σ_ε is, the larger the fluctuation of the porosity distribution becomes, and the results are shown in Fig. 3c.

In order to illustrate the flow field more clearly, the phenomena near the porous block are presented only. The region shown in the figure of the flow field is $1H_p$ upstream and $2.5H_p$ downstream from the porous block. As shown in Fig. 4, there are streamlines for different $\bar{\varepsilon}$ and σ_ε cases. The dimensionless stream function ψ is defined as

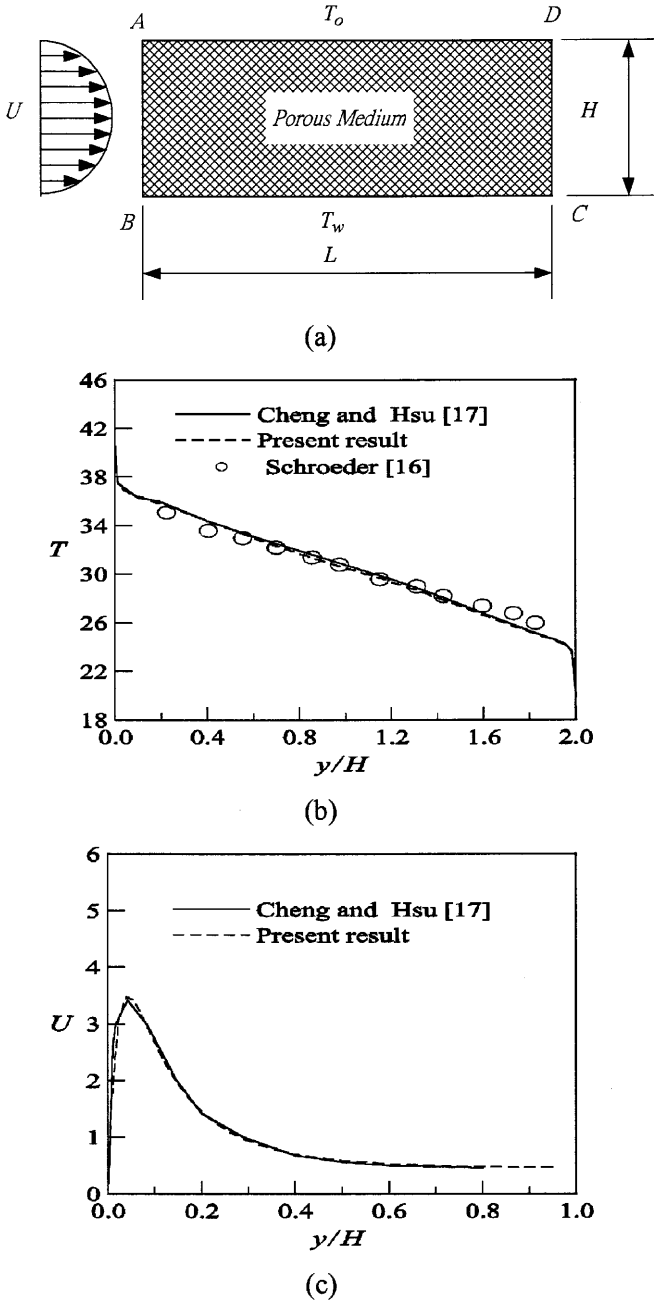

Fig. 2a–c. The comparisons between the results of Schroeder [16] and Cheng and Hsu [17] and this study under the variable porosity model. **a** Schematic diagram, **b** temperature distribution, **c** velocity distribution ($Re_p = 321$, $d_p/H = 0.37$, $\varepsilon = 0.4$, $k_s/k_f = 0.586$ and Pr = 7.0)

$$U = \frac{\partial \psi}{\partial Y} \quad \text{and} \quad V = -\frac{\partial \psi}{\partial X} \tag{19}$$

In Fig. 4a, two recirculation zones are found in both the upstream and downstream regions of the porous block. Some fluids penetrate into the porous block, which results in the downstream recirculation zone hardly neighboring to the porous block. The result indicates the effect of flow resistance inside porous block. The flow resistance inside porous block is mainly dependent on the porosity of porous block. Therefore, the flow pattern of Fig. 4b is similar to Fig. 4a, this also means that the effect of the variation of

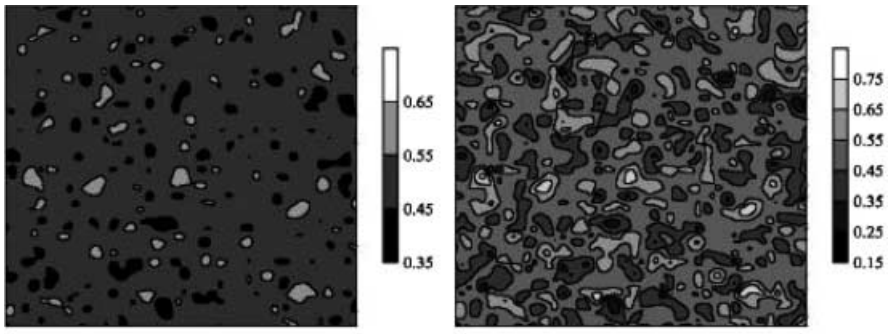

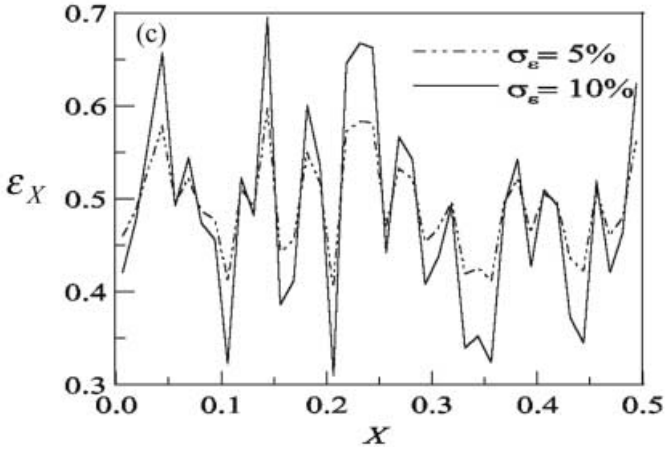

Fig. 3. **a** and **b** Global porosity distribution maps. **c** The local porosity ε_X distribution at $Y = 0.25$ along the X direction for $\bar{\varepsilon} = 0.5$ cases

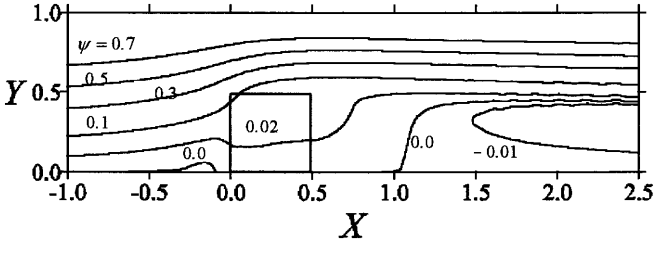

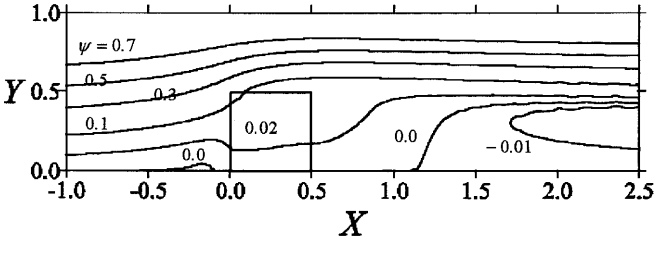

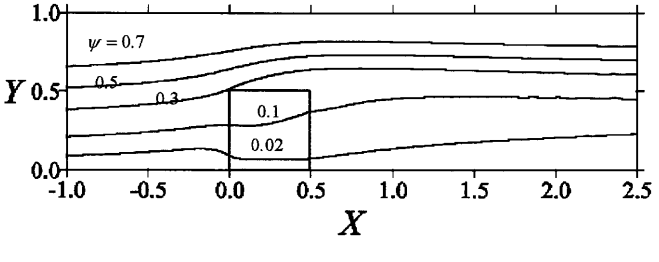

standard deviation on the flow field is slight. When $\bar{\varepsilon}$ becomes larger (=0.7) as shown in Fig. 4c, the streamline of $\psi = 0.02$ is close to the hot plate, which means more fluids to flow through the near wall region easily, and the recirculation zone forms further downstream, and the recirculation zone is hardly observed in the upstream region. The results point out the larger porosity accompanying with the smaller flow resistance inside the porous block.

In Fig. 5a, the variations of the velocity distributions of U at the middle position $(X = 0.25)$ of the porous block are illustrated. Due to the drastic variations of the porosity, the variations of local velocity U present jagged profiles and the channelling effect does not appear. For the different standard deviations σ_ε (=5%, 10%) under the same $\bar{\varepsilon}$ (=0.5) cases, the distributions of local velocity U are some different. As the mean porosity $\bar{\varepsilon}$ is larger, more fluids may flow through the porous block, and the distribution of local velocity U becomes larger. In Fig. 5b, the values of local velocity V are negative near the front edge of the block and positive near the back edge of the block, this indicates most fluids flow downward into the porous block and flow upward through out the block.

The local Nusselt number Nu and the average Nusselt number $\overline{\mathrm{Nu}}$ on the hot plate are defined as follows, respectively.

$$\mathrm{Nu} = \frac{h_x h}{k_\mathrm{f}} = -\frac{k_\mathrm{e}}{k_\mathrm{f}} \frac{\partial \theta}{\partial Y}\bigg|_{Y=0} \tag{20}$$

Fig. 4a–c. Streamlines of different cases: **a** $\bar{\varepsilon} = 0.5$, $\sigma_\varepsilon = 10\%$, **b** $\bar{\varepsilon} = 0.5$, $\sigma_\varepsilon = 5\%$, **c** $\bar{\varepsilon} = 0.7$, $\sigma_\varepsilon = 10\%$

$$\overline{\mathrm{Nu}} = \frac{1}{L_\mathrm{p}} \int_0^{L_\mathrm{p}} \mathrm{Nu}\, \mathrm{d}X \qquad (21)$$

Comparing with the cases of installing a solid block made of copper and without porous block in Fig. 6, the heat transfer rates are apparently enhanced for both $\bar{\varepsilon} = 0.5$ and 0.7 cases. The higher velocity U is attained for the $\bar{\varepsilon} = 0.7$ case (Fig. 5a), the values of Nu for $\bar{\varepsilon} = 0.7$ cases are then larger than those for the $\bar{\varepsilon} = 0.5$ cases. For the porous block cases, the fluids easily flow into the porous block, and the results show that the maximum Nusselt number appears in the front of porous block. For the solid block case, because of the high conductivity of copper and existence of flow separation in the front region, the distribution of local Nusselt number is flatter and more uniform than those of the porous block cases. In Table 3, the average Nusselt number $\overline{\mathrm{Nu}}$ of the solid block case is larger than those of $\bar{\varepsilon} \leq 0.4$ cases which indicates the small mean porosity porous block is able to reduce the heat transfer. The result means the fluids difficultly to flow into the porous block under the smaller mean porosity cases. Besides, the effect of standard deviation σ_ε on the local Nusselt numbers is very small and the results are shown in Fig. 6b.

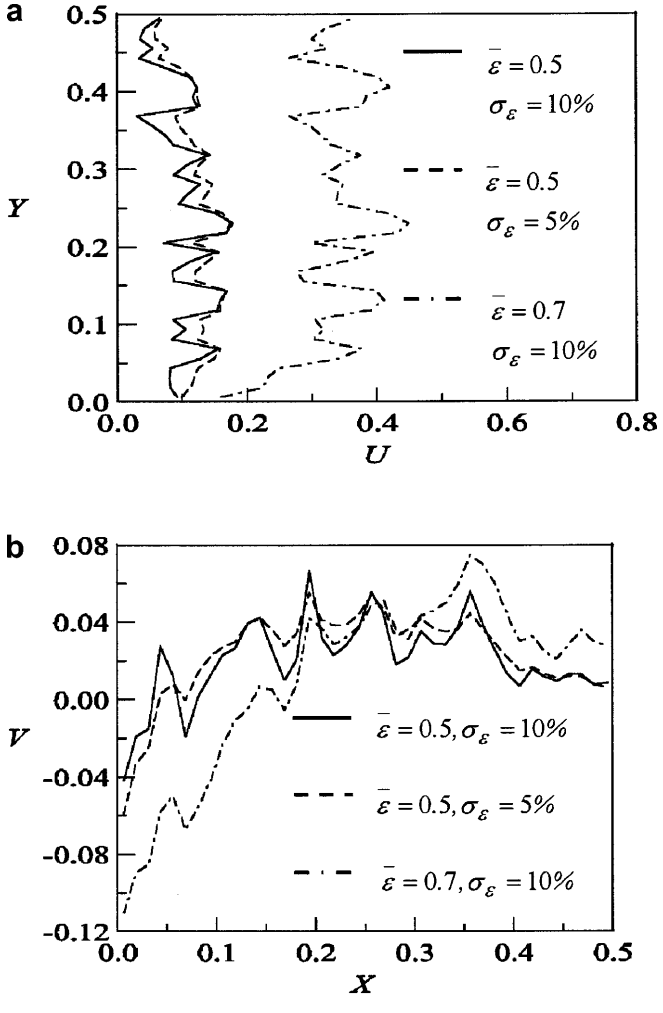

Fig. 5. **a** The profiles of velocity U at $X = 0.25$. **b** The profiles of velocity V at $Y = 0.25$

4.2
Effects of the artificial porosity model

Based upon the results of the above situations, the more fluids flow through the region close to the hot plate, the more heat transfer rate of the hot plate can be obtained.

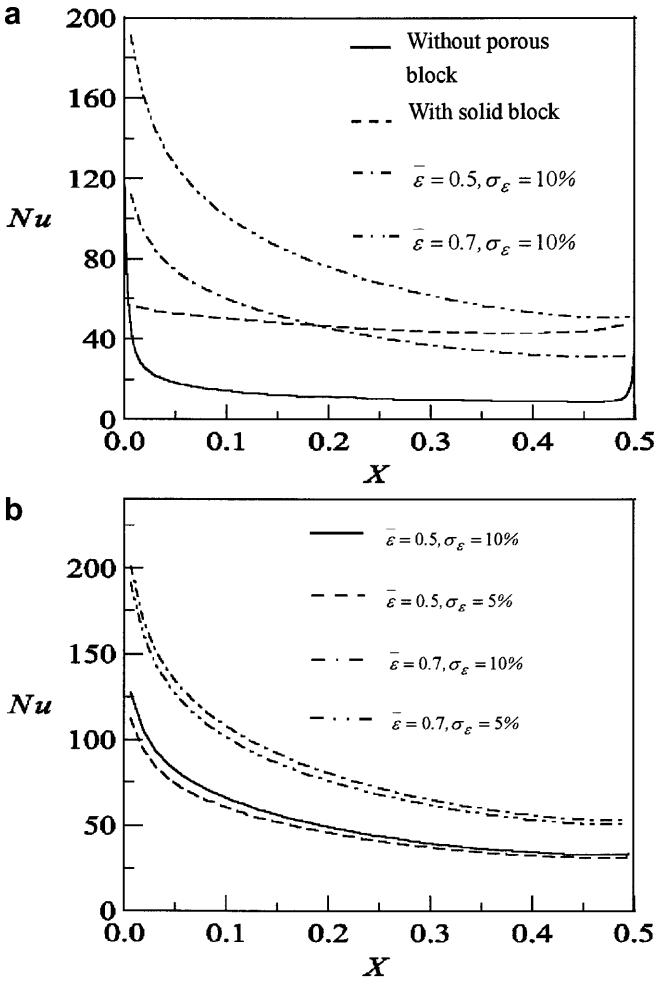

Fig. 6a, b. The distributions of local Nusselt number Nu for different conditions. **a** Comparison with the solid block and without porous block. **b** Comparison with the different standard deviations σ_ε

Table 3. The average Nusselt numbers of the different mean porosity cases based on artificial case A and the random porosity model under Re = 500, $\sigma_\varepsilon = 10\%$ and Pr = 0.7

$\bar{\varepsilon}$	$\overline{\mathrm{Nu}}$	
	Artificial porosity model (case A)	Random porosity model
0.0 (solid)	46.85	
0.2	22.32	
0.3	28.54	
0.4	40.82	
0.5	58.76	53.372
0.6	79.65	
0.7	100.65	85.964
0.8	118.02	
1.0 (blank)	13.20	

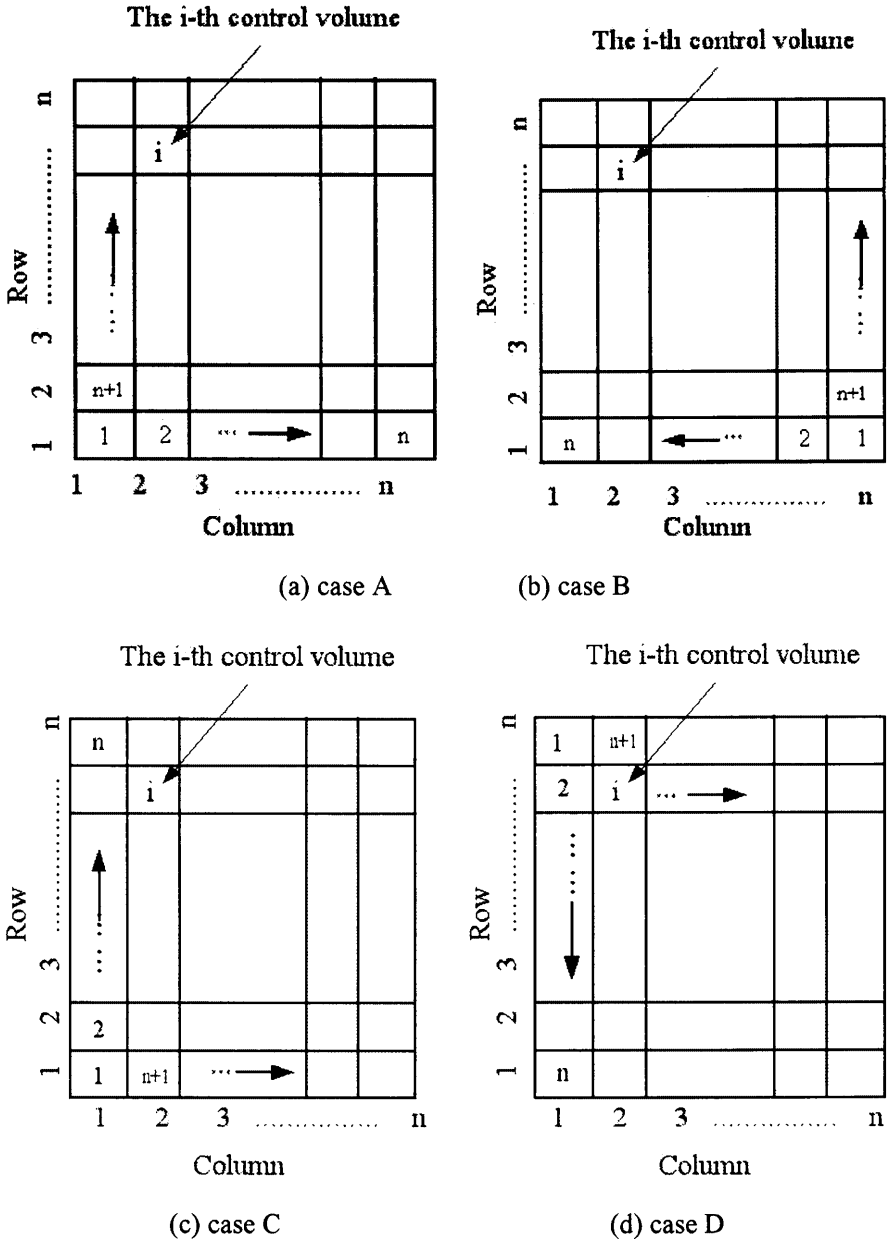

Fig. 7a–d. The arranging criteria of different artificial porosity models

Therefore, from a viewpoint of heat transfer enhancement, it is necessary to propose an available model which intentionally arranges a porosity on an appropriate position in a porous block to lead more fluids to flow near a hot plate. This method is briefly called as artificial porosity model. Four different arrangements of porosity block (A–D cases) derived by the artificial model are shown as follows.

The distribution of total porosities follows a normal distribution mentioned above. The porosity arranged by the artificial method in each case obeys the following rules, in which the sparsest porosity is arranged at the control volume 1 shown in Fig. 7. The larger number is the denser porosity becomes. Along the direction of the sign "$\rightarrow$", the porosity becomes denser. The porosity of the $(n+1)$th control volume is right behind that of (n)th control volume in the order of density. Four cases (A–D cases) with the artificial porosity model based on Re $= 500$, $\bar{\varepsilon} = 0.5, 0.7$, $\sigma_\varepsilon = 5\%, 10\%$, $D_\mathrm{p} = 0.1$, $\mathrm{Pr_f} = 0.7$ are calculated.

The global porosity distribution maps and the distribution of local porosity ε_X along the X direction are indicated in Fig. 8a and b, respectively, which are rather different from those of the random porosity model shown in Fig. 3a and b.

The streamlines of artificial cases A and C are illustrated in Fig. 9a and b, respectively. The streamlines of $\psi = 0.02$ of the artificial cases A and C are closer to the hot plate than those of the above cases shown in Fig. 4a and b. This indicates more fluids to flow through the region close to the hot plate and it is advantageous to the heat transfer rate of the hot plate.

As shown in Fig. 10, the velocity distributions of U (at $X = 0.25$) and V (at $Y = 0.25$) of the porous block are illustrated, respectively. Due to the rearrangement of porosity, the variation of the local porosity becomes small

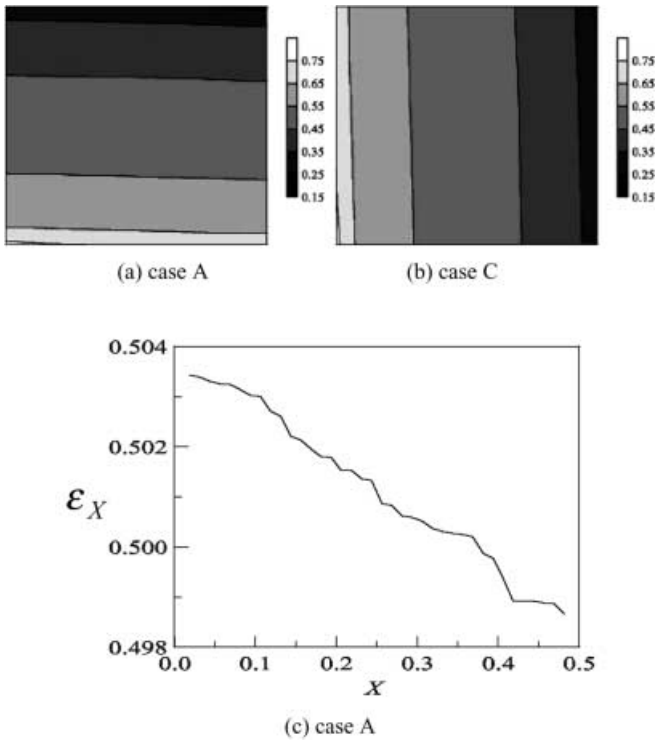

Fig. 8. **a** and **b** Global porosity distribution maps. **c** Distribution of local porosity at $Y = 0.25$ along the X direction

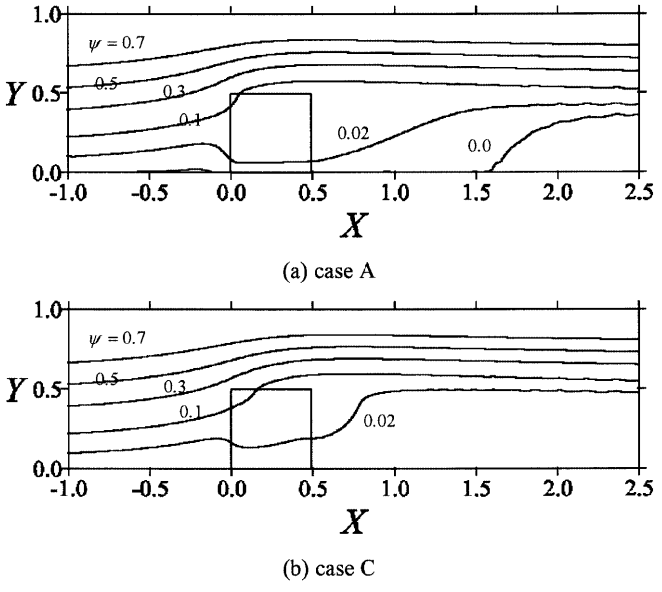

Fig. 9. Streamlines of different artificial cases based on $\bar{\varepsilon} = 0.5$

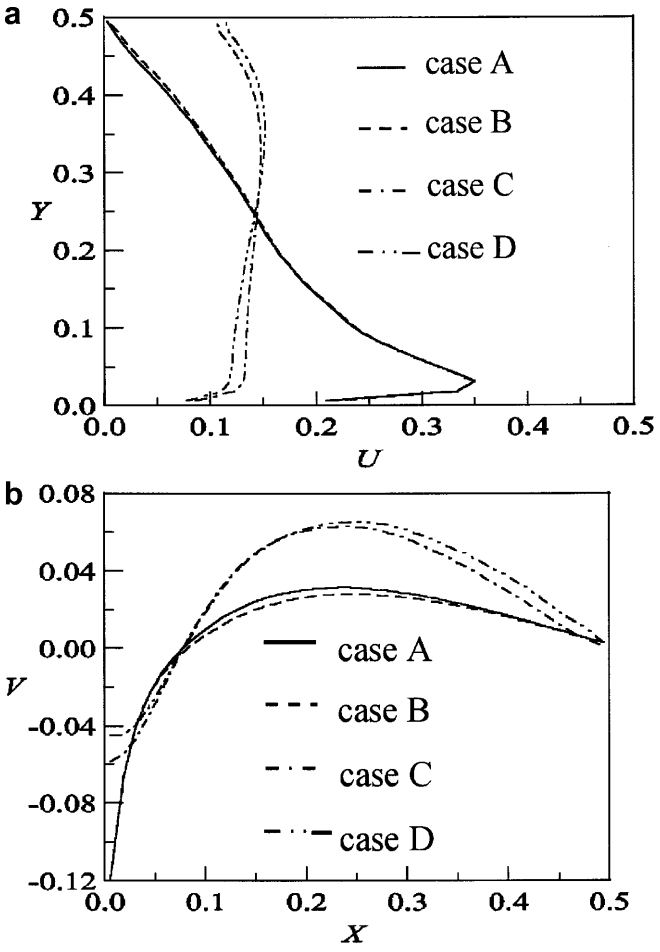

Fig. 10a, b. The velocity profiles of **a** U at $X = 0.25$ and **b** V at $Y = 0.25$ for the artificial porosity model

which causes the variations of the velocity distributions of U and V to be smooth. The channelling effect appearing in the artificial cases A and B is mainly affected by the sparser porosity distributed near the bottom, and based upon the same reason the fluids easily flow into the porous block which results in the values of velocity V being negative in most regions. In the artificial cases C and D, the sparse and dense porosities control volume are separately arranged in the front and rear edges of the porous block which causes the uniform profiles of the velocity U to happen and the values of the velocity V to be positive. According to the arrangement of the porosity mentioned above, the distributions of local velocities U and V of the artificial cases A and B are similar, and small difference exists between the artificial cases C and D.

The distributions of the local Nusselt number Nu attained by the artificial cases A, B, C, D and the random porosity model on the hot plate along the X direction are shown in Fig. 11. The values of Nu of the artificial cases A and B are larger than those of the cases C and D, and this means more fluids of the cases A and B to flow near the hot plate mentioned above. Besides, the local Nusselt numbers for the random porosity model are smaller than those of cases A and B, but better than those of cases C and D. Doubtless, the intentional arrangement of porosity is able to increase the heat transfer performance of hot plate. The average Nusselt numbers $\overline{\mathrm{Nu}}$ of different mean porosities and the random porosity model tabulated in Table 3. The value of "0.0" of the porosity means the porous block to be a solid block. As the mean porosity $\bar{\varepsilon}$ is larger than 0.5, the values of $\overline{\mathrm{Nu}}$ of porous block are larger than that of the solid one. This means that the use of porous block that used as a pin fin type dissipation device has a limitation.

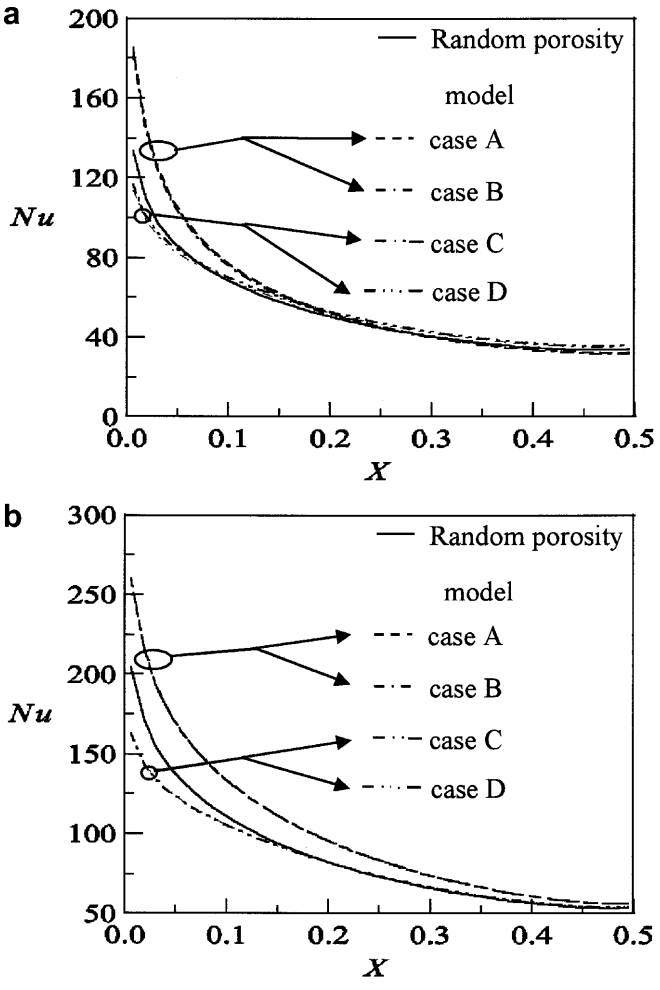

Fig. 11a, b. The distributions of local Nusselt number Nu on the hot plate for the random and artificial porosity models. **a** $\bar{\varepsilon} = 0.5$ and $\sigma_\varepsilon = 10\%$. **b** $\bar{\varepsilon} = 0.7$ and $\sigma_\varepsilon = 10\%$

5 Conclusion

The thermal performance of porous block mounted on the hot plate in a laminar channel flow with the random/artificial porosity models is numerically investigated. To enhance the thermal performance, the porous block with a higher thermal conductivity ratio (k_s/k_f) is adopted to simulate a heat sink.

The main results indicate that the porous block under the larger porosity situation $\bar{\varepsilon} \geq 0.5$ could obtain the thermal enhancement. For the random porosity model, the distributions of velocities U and V are chaotic and disorder. As for the artificial porosity model, the distributions of velocities U and V are smooth. The channelling effect is induced by the sparser porosities distributed near the hot plate apparently.

With the appropriate arrangement of the porosities, more fluids could flow through the region close to the hot plate, thus larger heat transfer rate of the hot plate can be obtained. Therefore, the porosity of porous block is artificially arranged like case A, the larger heat transfer rate can be expected.

References

1. **Roblee LHS; Baird RM; Tierney JW** (1958) Radial porosity variations in packed beds. AIChE J 4: 460–464
2. **Benenati RF; Brosilow CB** (1962) Void fraction distribution in packed beds. AIChE J 8: 359–361
3. **Schwartz CE; Smith JM** (1952) Flow distribution in packed beds. Indust Eng Chem 45: 1209–1218
4. **Cheng P; Chowdhury A; Hsu CT** (1991) Forced convection in packed tubes and channels with variable porosity and thermal dispersion effects. In: Kaka S et al. (eds) Convective Heat Mass Transfer in Porous Media, pp. 625–653
5. **Georgiads JG; Catton I** (1987) Stochastic modeling of unidirectional fluid transport in uniform and random packed beds. Phys Fluids 30: 1017–1022
6. **Catton I; Georgiads JG; Adnani P** (1988) The impact of nonlinear convective processes on transport phenomena in porous media. Proc 1988 National Heat Transfer Conference 1, ASME HTD-96, Houston, pp. 767–777
7. **Georgiads JG** (1991) Effect of randomness on heat and mass transfer in porous media. In: Kaka S et al. (eds) Convective Heat Mass Transfer in Porous Media, pp. 499–524
8. **Saito A; Okawa S; Suzuki T; Maeda H** (1995) Calculation of permeability of porous media using direct simulation Monte Carlo method. Proc ASME/JSME Thermal Engineering Joint Conference 3, Maui, pp. 297–304
9. **Fu WS; Huang HC** (1997) Thermal performances of different shape porous blocks under an impinging jet. Int J Heat Mass Transfer 40: 2261–2272
10. **Vafai K** (1984) Convective flow and heat transfer in variable-porosity media. J Fluid Mech 147: 233–259
11. **Batchelor GK; O'Brien RW** (1977) Thermal or electrical conduction through a granular material. Proc Royal Soc London, Series A: Mathematical and Physical Sciences 355: 313–333
12. **Shonnard DR; Whitaker S** (1989) The effective thermal conductivity for point contact porous medium: an experimental study. Int J Heat Mass Transfer 23: 503–512
13. **Hadim A** (1994) Forced convection in a porous channel with localized heat sources. J Heat Transfer 116: 465–472
14. **Fu WS; Huang HC** (1999) Effects of a random porosity model on heat transfer performance of porous media. Int J Heat Mass Transfer 42: 13–25
15. **Kennedy WJ; Gentle JE** (1980) Statistical Computing. Marcel Dekker, New York
16. **Schroeder KJ; Renz V; Elegeti K** (1981) Forschungsberichte des landes nordrhein-westfalen, Nr. 3037
17. **Cheng P; Hsu CT** (1986) Applications of Van Driest's mixing length theory to transverse thermal dispersion in a packed-bed with boundary walls. Int Comm Heat Mass Transfer 13: 613–625
18. **Fu WS; Huang HC; Liou WY** (1996) Thermal enhancement in laminar channel flow with a porous block. Int J Heat Mass Transfer 39: 2165–2175